

# Low-Resistivity Long-Length Horizontal Carbon Nanotube Bundles for Interconnect Applications—Part II: Characterization

Hong Li, *Member, IEEE*, Wei Liu, *Member, IEEE*, Alan M. Cassell, Franz Kreupl, *Member, IEEE*, and Kaustav Banerjee, *Fellow, IEEE*

**Abstract**—Due to the enormous challenges of fabricating long horizontally aligned carbon nanotube (HACNT) bundle interconnects, there exists little research on characterization of long HACNT interconnects. In this paper, taking advantage of our unique HACNT fabrication process outlined in the companion paper, the electrical and self-heating characterization of long HACNT bundles are reported. Negative temperature coefficients of resistance for both per unit length resistance and metal-CNT contact resistance are confirmed from measurements. This first report on the electrical and thermal characterization fills the wide gap between CNT interconnect modeling efforts and corresponding experimental efforts by providing many important extracted parameters that are critical in various modeling and analyses.

**Index Terms**—Carbon nanotubes, characterization, horizontally aligned, interconnects, resistivity, self-heating, temperature coefficient of resistance.

## I. INTRODUCTION

CARBON NANOTUBES (CNTs) have been proposed as a promising material to replace Cu for both horizontal and vertical interconnects as well as passive devices (such as inductors) to address performance and reliability concerns for next-generation electronics [1]–[6]. During the past decade, there has been a lot of progress in experimental process development for CNT interconnects, however, most of the fabrication efforts have been directed toward vertical vias, such as low-resistance and high-density CNT bundle vias [7], [8], and integration of CNT vias with ultra low- $k$  dielectric [9]. This is primarily because of the relative ease with which short ( $<1 \mu\text{m}$ ) CNTs can be vertically grown in predefined trenches. Nevertheless, it has been always very challenging

Manuscript received February 8, 2013; revised July 13, 2013; accepted July 15, 2013. Date of current version August 19, 2013. This work was supported by the National Science Foundation under Grant CCF-0811880. The review of this paper was arranged by Editor A. C. Seabaugh.

H. Li was with the Department of Electrical and Computer Engineering, University of California, Santa Barbara, CA 93106 USA. He is now with Emerging Memory Group, Micron Technology, Boise, ID 83707 USA (e-mail: hongli@micron.com).

W. Liu and K. Banerjee are with the Department of Electrical and Computer Engineering, University of California, Santa Barbara, CA 93106 USA (e-mail: liuwei@ece.ucsb.edu; kaustav@ece.ucsb.edu).

A. M. Cassell is with NASA Ames Research Center, Moffett Field, CA 94035 USA (e-mail: alan.m.cassell@nasa.gov).

F. Kreupl is with the Department of Hybrid Electronic Systems, Technische Universität München 80333, Germany (e-mail: franz.kreupl@tum.de).

Color versions of one or more of the figures in this paper are available online at <http://ieeexplore.ieee.org>.

Digital Object Identifier 10.1109/TEDE.2013.2275258

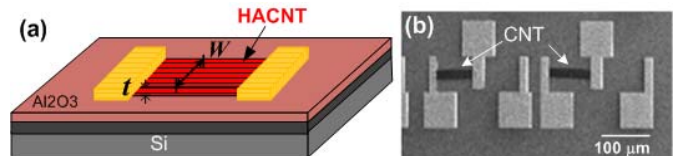


Fig. 1. (a) Schematic view and (b) SEM image of the fabricated HACNT test structure. Substrate consists of 20-nm  $\text{Al}_2\text{O}_3$  on top of 100-nm  $\text{SiO}_2$  lying over low-doped silicon.

to fabricate long horizontal CNT interconnects, even though they are the most commonly studied structure in modeling works [4], [5], [10]–[12]. Because of the lack of horizontally aligned CNT (HACNT) fabrication process and structures, there is little research on characterization of HACNT bundles that are suitable for interconnect application.

Recently, we have developed a process that allows us to fabricate long (over  $100 \mu\text{m}$ ) HACNT bundle interconnects by flattening vertically aligned CNT (VACNT) bundles using liquid-assisted flattening technique (Part I of this paper, [13]). Taking advantage of the developed process, arrays of HACNT bundle interconnect test structures are fabricated with various width, thickness, and length of HACNTs (shown in Fig. 1). In this paper, the electrical and thermal (self-heating) characterization of long HACNT bundles are reported for the first time. The reported electrical and thermal characterization fills the wide gap between CNT interconnect modeling efforts and corresponding experimental efforts by providing many important extracted parameters that are critical in various modeling and analyses.

The paper is organized as follows. Section II first compares the extracted resistance with existing reported values and also discusses the pathways for further improvement. Section III discusses the impact of pressure and temperature on the resistance of HACNT bundles and extracts their temperature coefficient of resistance (TCR). The self-heating effect of HACNT bundles and their corresponding temperature rise are studied in Section IV. Finally, Section V draws the conclusions.

## II. RESISTIVITY OF HACNT BUNDLES

### A. Resistivity Extraction

With various lengths of HACNT interconnects, one can extract the per unit length resistance ( $R_{p,u,l}$ ) of CNT

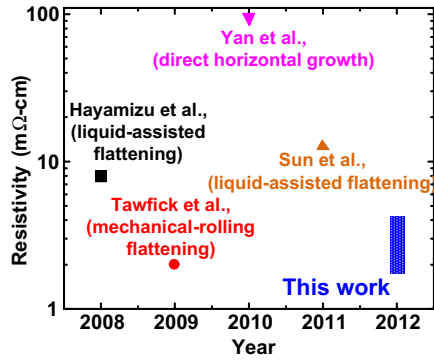


Fig. 2. Extracted HACNT resistivity compared with other reports in literature [14]–[17], showing that lowest resistivity has been achieved.

interconnect using transmission line measurement (TLM), as well as its effective resistivity ( $\rho$ ) for a given interconnect width ( $W$ ) and thickness ( $t$ ) using  $\rho = R_{p.u.l} \cdot W \cdot t$ . Note that  $t$  is the thickness of HACNT after flattening. The thickness ratio before and after densification of CNT bundles is defined as densification ratio  $D_R = T/t$ , which is process dependent. For the process used in this paper,  $D_R$  is  $\sim 45$  as shown in Fig. 5 of Part I [13], where  $t \sim 220$  nm for an HACNT that initially (in the form of VACNT) has  $T = 10$   $\mu\text{m}$ . Assuming  $D_R = 45$ , the resistivity of HACNT interconnects is calculated to be in the range of 1.7–4.1 m $\Omega$ -cm. Fig. 2 shows the resistivity comparison with other reports in literature [14]–[17]. It is instructive to note that the direct growth technique reported in [14], resulted in relatively sparse and short-length CNT bundles (<2- $\mu\text{m}$ -long interconnect was demonstrated). Although the flattening technique was first demonstrated in [15] using liquid assistance, and then followed by [16], [17], our fabrication process overcomes several challenging issues in the flattening process that are crucial for very large scale integration (VLSI) applications, such as enabling the fabrication of long length, thick HACNT bundles with relatively small widths, formation of full metal HACNT contacts, as well as the first demonstration of 2-D Manhattan structures that are important for designing angled interconnects and passive structures such as spiral inductors (details can be found in Part I [13]). The resistivity we achieved is the lowest for horizontal multiwalled CNT bundles reported till date. In addition to resistivity, the contact resistivity (contact resistance normalized to per unit catalyst area) of our structure is between  $6 \times 10^{-5}$   $\Omega\text{-cm}^2$  and  $2 \times 10^{-4}$   $\Omega\text{-cm}^2$ , which are several times lower than the previously reported value of  $5 \times 10^{-4}$   $\Omega\text{-cm}^2$  in [17]. Note that the actual contact resistivity will be  $\sim 45$  times smaller in our cases (on the order of  $10^{-6}$   $\Omega\text{-cm}^2$ ), since the actual HACNT cross-sectional area is  $\sim 45$  times smaller than the catalyst area.

To compare the resistivity with that of a metal, we also fabricated and measured the same TLM-like structures made from 500-/1500-nm Ti/Au interconnects. The extracted resistivity for Ti/Au metal line is  $0.032 \pm 0.001$  m $\Omega$ -cm. Hence, even though our fabricated CNT interconnect is the best among existing reports, it is still nearly two orders larger than that of metal interconnects, indicating that significant improvement is

needed. It should be, however, pointed out that the developed alignment procedure HACNT is also applicable to supergrowth structures of single-walled nanotubes [15]. In the case of nanotube spun fibers, a record low resistivity of only 17.5  $\mu\Omega$ -cm has been achieved recently [18], which is well compatible or even better than traditional metallization schemes.

It is instructive to note that this paper is the first demonstration that one can fabricate reasonably long and comprehensive test structures for CNT bundle-based interconnects. The scalability of our fabrication process has been discussed in [13]. The capability of fabricating such large and long interconnect structures provides the foundation for many interesting and important experiments where the structure sizes need not be nanoscale. For instance, it allows one to measure the inductive behavior of CNT bundle structures for their application as inductors coils, and to calibrate the theoretical analysis as shown in [19]. This paper represents the first step toward the fabrication of these structures and in understanding their basic electrical properties.

### B. Resistivity Improvement Pathways

There are many ways to further improve the resistivity of HACNT bundles in future work. The resistivity of HACNTs can be calculated from

$$\rho_{\text{HACNT}} = \frac{1}{G_{\text{CNT}} \cdot N_{\text{CNT}}} \quad (1)$$

where  $G_{\text{CNT}}$  is the conductivity of individual CNT and  $N_{\text{CNT}}$  is the number of CNTs/unit area. Hence, two major directions can be pursued to improve  $\rho_{\text{HACNT}}$ : 1) increase the conductivity of individual CNT and 2) increasing the packing density of the bundle.

On the aspect of reducing the resistivity of individual CNTs, the CVD growth can be improved further to achieve low-defect high-quality CNT growth. For MWCNTs, achieving more shells for a given outermost diameter would be very helpful. In this paper, the grown CNTs are mostly three and four shells with diameter of 6–8 nm [13, Fig. 4] [17], indicating that  $\sim 2/3$  of the space inside a MWCNT is empty, which obviously is not good for achieving low resistivity [11]. In addition, growing higher fraction of metallic shells is always critical (but extremely challenging) for achieving lower resistivity, both for MWCNTs and SWCNTs. Although there are some reports along such directions [20]–[22], further catalyst engineering and growth optimization will be needed. Recent work [18] on CNT fibers show that, there is still room for possible improvement even at the chip level.

On the aspect of increasing packing density, one can achieve this by increasing the density of *in situ* grown VACNT bundles, as well as by enhancing the densification ratio ( $D_R$ ) using postprocess techniques. Using the method proposed in [23], we roughly estimate the density of our VACNT to be  $3.6 \times 10^{10}$   $\text{cm}^{-2}$ , which is <2% of the volume fraction compared with an ideal densely packed CNT bundle, indicating that there is plenty of room for density improvement. Recently, Zhong *et al.* [24] has reported as-grown CNT density close to the dewetting limit through catalyst engineering, achieving  $1.5 \times 10^{13}$   $\text{cm}^{-2}$  for 1-nm diameter SWCNTs. Note that one of

the practical limitations to achieve high *in situ* growth density is that the catalyst nanoparticle formation is limited by the thin-film dewetting process, which has a thermodynamic limit (usually smaller than ideal CNT density) [20], [23]. To possibly overcome this limit, selective deposition of pregenerated catalyst nanoparticles instead of catalyst thin-film annealing has been reported in [25]. For postprocess densification, to further enhance the densification ratio, external forces (such as research in [16] and [26]) can be applied to reduce the empty spaces between CNTs. Finally, one can explore “metal-filled” CNT bundles as an alternative pathway for achieving low-resistivity.

### III. ENVIRONMENTAL IMPACT ON CNT RESISTANCE

#### A. Impact of Ambient Pressure

It is known that CNTs are sensitive to the environment, which is particularly good for sensor applications. Because of its large surface-area to volume ratio and low density of states, the properties of CNT can be easily modified by surface dopants from the ambient. For the structures we have fabricated, there is no encapsulation layer to isolate HACNT interconnects from the ambient, which provides an opportunity for us to study the impact of ambient pressure on its electrical resistance.

We first measured the samples under atmospheric condition, and then repeated the measurements under different vacuum conditions at room temperature. Fig. 3 shows the resistance measurement results for different HACNTs. It can be observed that as the pressure decreases, the resistance increases for all the HACNTs. This can be explained by the doping effect under ambient atmospheric conditions. At atmospheric pressure, molecules such as water and oxygen in the air can attach to the CNT surfaces, which effectively dope the CNTs and increase the carrier density of CNTs. Whereas under vacuum condition, these molecules are detached from the CNT surfaces and the doping effect is diminished, thereby increasing the resistance of CNTs.

After the above measurements, the samples were heated from room temperature to 410 K and subsequently cooled down to room temperature to be measured again. The resistance measurement after this heating is also shown in Fig. 3, where the resistance is observed to increase slightly. This is attributed to the fact that the molecular dopants are further removed at high temperatures. Because of the resistance change shown in Fig. 3, the conditioning under high vacuum and high temperature was performed in all the subsequent investigations before each evaluation, followed by the evaluation under vacuum. In this way, the impact of doping effects from the ambient can be eliminated to a large extent during the subsequent temperature-dependent measurements.

#### B. Impact of Temperature

To study the intrinsic properties of CNTs, all the temperature-dependent measurements in this paper were carried out under vacuum conditions (1E-5 mbar), so that the doping effect from ambient environment is minimal. It is to

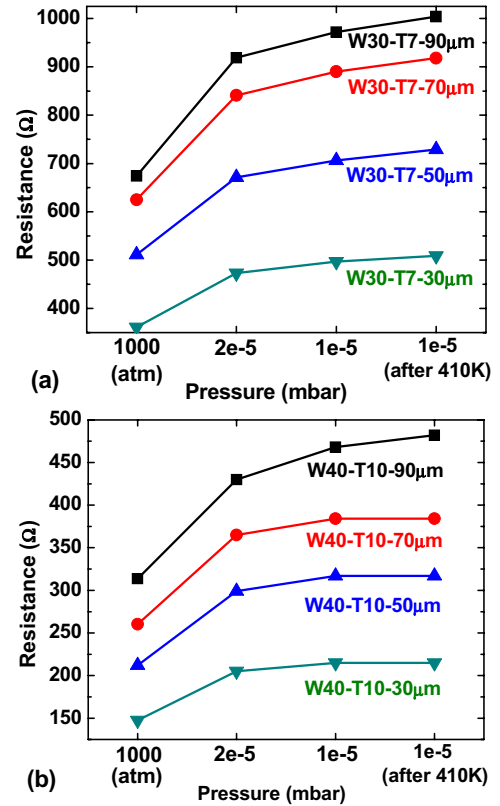


Fig. 3. Resistance of HACNT bundles (measured at room temperature) increases as the pressure decreases from the atmospheric (atm) value, for both (a) devices fabricated from  $W = 30 \mu\text{m}$ ,  $T = 7 \mu\text{m}$  (W30-T7) VACNTs and (b) devices fabricated from  $W = 40 \mu\text{m}$ ,  $T = 10 \mu\text{m}$  (W40-T10) VACNTs. Furthermore, if the devices are heated (for instance to 410 K and then cooled down to room temperature), the resistance also increases slightly at the same pressure.

be noted that HACNT interconnects lay on the substrate, and the surface charges from the substrate may play a role here.

Fig. 4 shows the resistance measurement of two sets of HACNT interconnects with different temperatures under vacuum. It is clearly observed that as temperature increases, the resistance decreases slightly for all the lengths. This indicates that the fabricated CNT bundles have negative TCR. Note that the measured resistance has two components: 1) scattering resistance ( $R_{p,u,l}$ ) and 2) contact resistance ( $R_{\text{cont}}$ ), following the relationship

$$R_{\text{meas}} = R_{p,u,l} \times L + 2R_{\text{cont}} \quad (2)$$

where  $L$  is the length of HACNT interconnects. With the data shown in Fig. 4, we can extract  $R_{p,u,l}$  and  $R_{\text{cont}}$  using (2) for a given temperature. Then, the TCR of both scattering resistance and contact resistance can be obtained using

$$R = R_0[1 + \text{TCR} \cdot (T - T_0)] \quad (3)$$

where  $R_0$  and  $T_0$  are the initial measured resistance and initial temperature, respectively.

Fig. 5 shows the extracted TCRs for two sets of devices as well as the TCRs for  $R_{p,u,l}$  and  $R_{\text{cont}}$ . All the extracted TCRs are negative, including that of contact resistance. The negative TCR is consistent with theoretical analysis [27], [28]

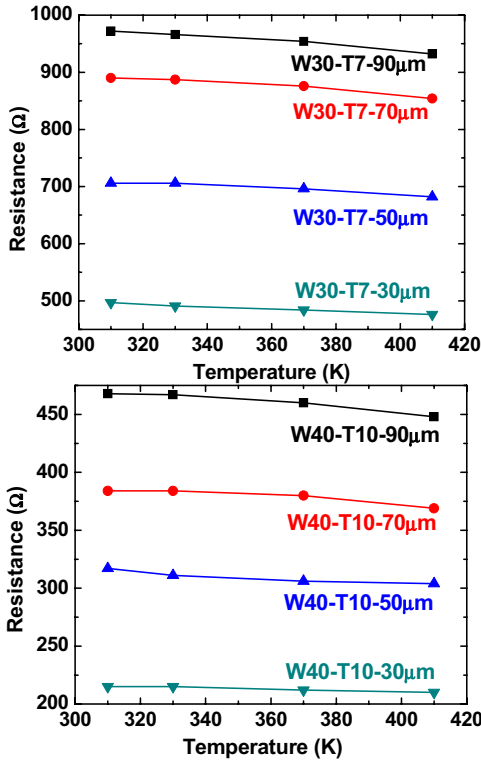


Fig. 4. Resistance of HACNT devices decreases as temperature increases, indicating negative temperature coefficient of resistance (TCR), for both (a) devices fabricated from  $W = 30 \mu\text{m}$ ,  $T = 7 \mu\text{m}$  (W30-T7) VACNTs and (b) devices fabricated from  $W = 40 \mu\text{m}$ ,  $T = 10 \mu\text{m}$  (W40-T10) VACNTs. All the measurements are carried out under vacuum condition ( $1\text{E-}5$  mbar) to eliminate the impact of ambient pressure as much as possible

as well as existing experimental reports [30] for MWCNTs.<sup>1</sup> It can be explained from the fact that there are more subbands in MWCNTs contributing to conductance at higher temperatures as per Fermi–Dirac distribution [11]. Larger number of conducting subbands lowers both scattering resistance and contact resistance. The negative TCR is opposite to that of traditional metal conductors, and could be an advantage for electronics applications as the operating temperature of advanced devices is mostly at several tens of degree celsius above room temperature [29].

#### IV. SELF-HEATING EFFECTS IN HACNT INTERCONNECTS

For interconnect applications, self-heating effect has significant implications as it affects both performance and reliability of the circuits, particularly for aggressively scaled VLSI [6], [29], [31]. Because of the lack of long CNT bundle fabrication process, little research has been, however, published on such characterization for CNT bundle interconnects. Our fabricated long HACNT structures offer unique opportunities to study the self-heating effect of CNT bundles.

For self-heating characterization, current is flown through the CNT interconnect structure and the resistance is then measured. Fig. 6 shows the resistance variations as a function of forced current. It can be observed that as current increases,

<sup>1</sup>TCR for CNTs is not necessarily negative. Particularly in case of SWCNTs, TCR is usually positive, as discussed in [6] and [27].

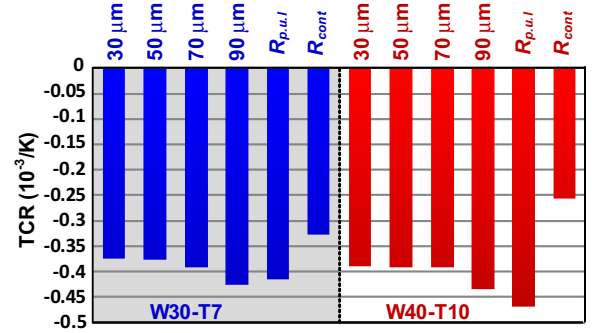


Fig. 5. Extracted TCRs for two sets of devices with different lengths. TCR of HACNT/unit length resistance ( $R_{p,u,l}$ ) and metal-CNT contact resistance ( $R_{cont}$ ) are also extracted from the data as shown in Fig. 4.

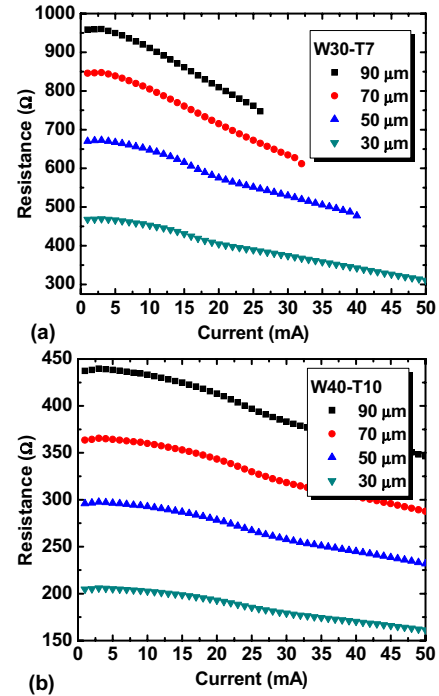


Fig. 6. Resistance of one set of HACNT devices as a function of forced current, for both (a) devices fabricated from  $W = 30 \mu\text{m}$ ,  $T = 7 \mu\text{m}$  (W30-T7) VACNTs and (b) devices fabricated from  $W = 40 \mu\text{m}$ ,  $T = 10 \mu\text{m}$  (W40-T10) VACNTs. Square, circle, up triangle, and down triangle legends represent CNT lengths 90, 70, 50, and  $30 \mu\text{m}$ , respectively.

the resistance of CNT structures decreases. This behavior can be explained by joule heating (or self-heating) effect and is consistent with the negative TCRs shown in Fig. 5. As current increases, joule heating-induced temperature increases and the resistance decreases due to negative TCR. Note that some of the data points in Fig. 6(a) could not be completed because of reaching voltage compliance during measurements.

Once the relationship between resistance and current is measured, using the already extracted TCR, we can estimate the temperature rise due to joule heating from

$$\Delta T = \frac{(R - R_0)}{\text{TCR} \cdot R_0}. \quad (4)$$

Fig. 7 shows the estimated temperature rise for different set of devices as a function of input current density. The current density is calculated using the densification ratio of

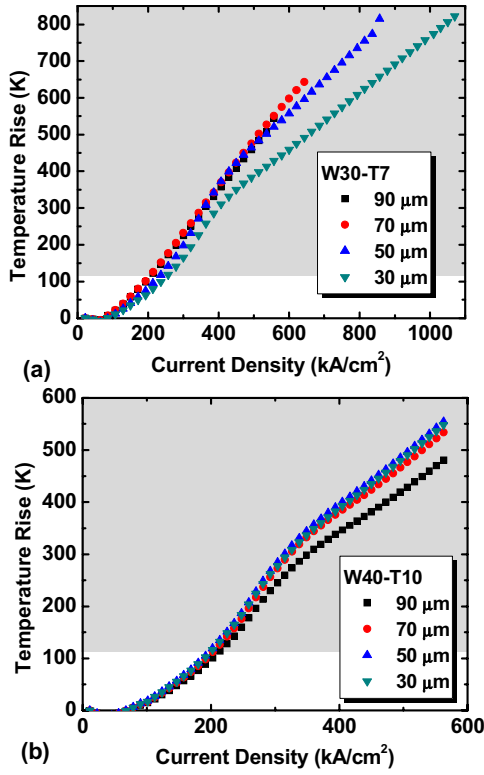


Fig. 7. Estimated temperature rise due to joule heating as a function of input current density, for both (a) devices fabricated from  $W = 30 \mu\text{m}$ ,  $T = 7 \mu\text{m}$  (W30-T7) VACNTs and (b) devices fabricated from  $W = 40 \mu\text{m}$ ,  $T = 10 \mu\text{m}$  (W40-T10) VACNTs. Square, circle, up triangle, and down triangle legends represent CNT lengths 90, 70, 50, and  $30 \mu\text{m}$ , respectively.

HACNT  $D_R = 45$ . It is observed that for a given current density, the temperature rise values for one set of devices with same width [ $30\text{-}\mu\text{m}$  width shown in Fig. 7(a) and  $40\text{-}\mu\text{m}$  width shown in Fig. 7(b)] are quite similar. This is not so intuitive at this moment, and will be explained later in this section. It is shown from Fig. 7 that no damage is observed for current density exceeding  $10^6 \text{ A/cm}^2$ . Note that the current did not go higher due to compliance setup of the measurement. It should also be noted that the packing density of the HACNT is estimated to be  $<5\%$  of ideal packing. For densely packed CNT bundles, the current density would be even higher, indicating excellent reliability potential for these HACNT.

Fig. 8 shows similar plots but now as a function of input power ( $I^2R$ ). As power increases, the temperature increase is slower for longer length CNT interconnects. This indicates that the substrate played a significant role as a heat sink. As the length of interconnect increases, the thermal interface between HACNT and substrate increases so that heat is dissipated more effectively. The metal contacts surely contribute to heat dissipation, but their contribution can be assumed to be constant for samples with different lengths. The fact that temperature rises are almost identical for different lengths indicates that the contact contribution to heat dissipation may not be the dominating factor, as explained below.

For a given power  $P$ , the temperature rise is  $\Delta T = P \cdot \Theta_{\text{th}}$ , where  $\Theta_{\text{th}}$  is the thermal resistance of the structure.

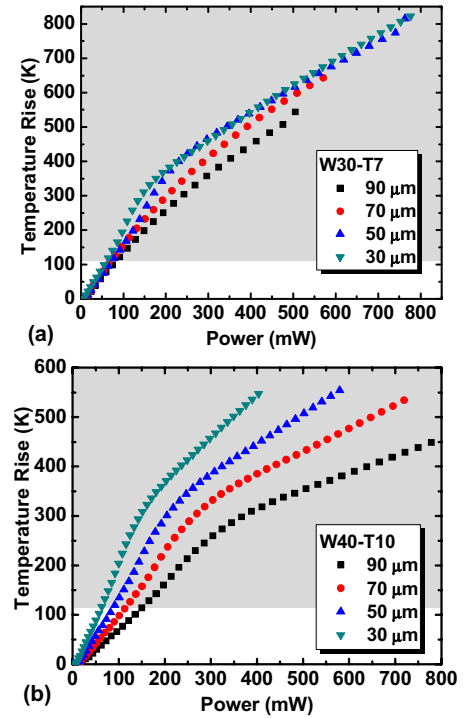


Fig. 8. Extracted temperature rise due to joule heating as a function of input power ( $I^2R$ ), for two sets of devices flattened from VACNTs with dimensions (a)  $W = 30 \mu\text{m}$ ,  $T = 7 \mu\text{m}$  (W30-T7) and (b)  $W = 40 \mu\text{m}$ ,  $T = 10 \mu\text{m}$  (W40-T10). Square, circle, up triangle, and down triangle legends represent CNT lengths 90, 70, 50, and  $30 \mu\text{m}$ , respectively.

By replacing  $P$  with  $I^2R$ , we can obtain

$$I^2R \cdot \Theta_{\text{th}} = J^2 A^2 R \cdot \Theta_{\text{th}} = \Delta T \quad (5a)$$

$$J^2 \cdot A \cdot \rho_{\text{CNT}} \cdot \Theta_{\text{th}} \cdot L = \Delta T \quad (5b)$$

where  $J$  is the current density,  $A$  is the cross-sectional area of HACNT (width  $W$  by thickness  $T$ ), and  $L$  is the length of HACNT.

$\Theta_{\text{th}}$  has two contributors: 1) substrate  $\Theta_{\text{sub}}$  and 2) metal-CNT contacts  $\Theta_{\text{cont}}$ . The first part  $\Theta_{\text{sub}}$  would be inversely proportional to  $L$  and the second part  $\Theta_{\text{cont}}$  would be independent of  $L$ . To explain the fact that  $\Delta T$  is independent of length,  $\Theta_{\text{th}}$  should be inversely proportional to  $L$  as indicated in (5b). Therefore, we could interpret Fig. 7 as an indication that the first heat dissipation contributor  $\Theta_{\text{sub}}$  from the substrate plays a major role here.

It should be noted that the slopes of the temperature rise curves in Fig. 8 decrease after  $\sim 275\text{--}300 \text{ K}$  of temperature rise. This could be partly because of the inaccuracy in TCR estimation for high temperatures. The TCRs are extracted from measurements in the temperature range 300 to 410 K. There is no TCR value for higher temperatures because of the limitations of our measurement setup. At very high temperatures, charge scattering probability increases and may overwhelm the benefit of having more conducting channels for MWCNTs, so that the TCR could become less negative. According to (3), less negative TCR indicates that the temperature rise values shown in Figs. 7 and 8 are underestimated. This explains why the temperature rise slows down in Figs. 7 and 8 at high temperatures. To be more precise, we mark the areas with temperature rise  $> 110 \text{ K}$  in Figs. 7 and 8 as gray regions

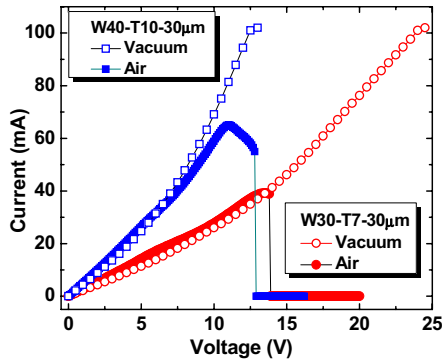


Fig. 9. Breakdown experiments on two devices showing that breakdown current significantly increases in vacuum and breakdown is not observed even with current exceeding the compliance limit of 100 mA (for W30-T7, current density  $>2.2 \times 10^6$  A/cm<sup>2</sup>).

to indicate that these regions are based on our theoretical prediction as we did not have actual measured TCR data.

We also measured the breakdown current of our samples. Fig. 9 shows breakdown measurement under both air and vacuum conditions for two differently sized CNT interconnects. The observed negative TCR at low temperature shows up in the nonlinear part of the  $I$ - $V$  curve in Fig. 9. At stress currents  $>50$  mA, the  $I$ - $V$  curve is more linear, which would confirm the disappearance of negative TCR. We can observe that the breakdown current is significantly higher in vacuum. Within the current compliance limit (100 mA) of our measurement setup, we did not observe any breakdown event, which indicates that the breakdown current density exceeds  $2.2 \times 10^6$  A/cm<sup>2</sup> (the current density of Cu is also on the order of  $10^6$  A/cm<sup>2</sup>). When the same samples were measured again in atmosphere, the breakdown happened at a current density of  $\sim 8.4 \times 10^5$  A/cm<sup>2</sup> for W30-T7 and  $7.4 \times 10^5$  A/cm<sup>2</sup> for W40-T10. Since it is difficult to characterize the TCR in atmosphere due to doping effects as described in Section III-A, an accurate self-heating analysis was not feasible. However, for simplicity, if we assume that the trend is the same as in Fig. 7, we can roughly estimate the breakdown temperature to be  $\sim 667$  °C (with  $\sim 640$ -K temperature rise) for the case of W30-T7. This temperature agrees surprisingly well with breakdown temperature determinations ( $600$  °C  $\pm$   $100$  °C) by thermogravimetric analysis [32], [33].

## V. CONCLUSION

In this paper, the electrical and self-heating characterization of long HACNT bundles are reported for the first time. The fabricated several tens of micrometer long HACNTs achieved the lowest reported resistivity to date. The pressure dependence of resistivity is also observed and explained by the ambient doping effect. Negative TCRs were confirmed from measurement, from both HACNT's per unit length resistance and metal-CNT contact resistance. Self-heating characterization also shows no damage for current density exceeding  $2.2 \times 10^6$  A/cm<sup>2</sup> even though the HACNT bundles were sparsely packed ( $<5\%$  filling factor), indicating great potential for interconnect reliability.

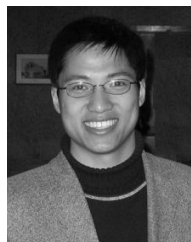
## ACKNOWLEDGMENT

All process steps for device fabrication were carried out using the Nanostructure Cleanroom Facility at the California NanoSystems Institute and the Nanofabrication Facilities at UCSB - part of the National Nanotechnology Infrastructure Network. K. B. thanks the Alexander von Humboldt Foundation in Germany for the F. W. Bessel Research Award that greatly facilitated many stimulating discussions with F. K. in München.

## REFERENCES

- [1] J. Hone, M. Whitney, C. Piskoti, and A. Zettl, "Thermal conductivity of single-walled carbon nanotubes," *Phys. Rev. B*, vol. 59, no. 4, pp. R2514–R2516, Jan. 1999.
- [2] B. Q. Wei, R. Vajtai, and P. M. Ajayan, "Reliability and current carrying capacity of carbon nanotubes," *Appl. Phys. Lett.*, vol. 79, pp. 1172–1174, Aug. 2001.
- [3] F. Li, H. M. Cheng, S. Bai, G. Su, and M. S. Dresselhaus, "Tensile strength of single-walled carbon nanotubes directly measured from their macroscopic ropes," *Appl. Phys. Lett.*, vol. 77, no. 20, pp. 3161–3163, 2000.
- [4] N. Srivastava, H. Li, F. Kreupl, and K. Banerjee, "On the applicability of single-walled carbon nanotubes as VLSI interconnects," *IEEE Trans. Nanotechnol.*, vol. 8, no. 4, pp. 542–559, Jul. 2009.
- [5] H. Li, C. Xu, and K. Banerjee, "Carbon nanomaterials: The ideal interconnect technology for next-generation ICs," *IEEE Design Test Comput.*, vol. 27, no. 4, pp. 20–31, Jul./Aug. 2010.
- [6] H. Li, N. Srivastava, J.-F. Mao, W.-Y. Yin, and K. Banerjee, "Carbon nanotube vias: Does ballistic electron and phonon transport imply improved performance and reliability?" *IEEE Trans. Electron Devices*, vol. 58, no. 8, pp. 2689–2701, Aug. 2011.
- [7] M. Nihei, T. Hyakushima, S. Sato, T. Nozue, M. Norimatsu, M. Mishima, T. Murakami, D. Kondo, A. Kawabata, M. Ohfuti, and Y. Awano, "Electrical properties of carbon nanotube via interconnects fabricated by novel damascene process," in *Proc. IEEE IITC*, Jan. 2007, pp. 204–206.
- [8] J. Dijon, H. Okuno, M. Fayolle, T. Vo, J. Pontcharra, D. Acquaviva, D. Bouvet, A. M. Ionescu, C. S. Esconjauregui, B. Capraro, E. Quesnel, and J. Robertson, "Ultra-high density carbon nanotubes on Al-Cu for advanced vias," in *IEDM Tech. Dig.*, 2010, pp. 33.4.1–33.4.4.
- [9] A. Kawabata, S. Sato, T. Nozue, T. Hyakushima, M. Norimatsu, M. Mishima, T. Murakami, D. Kondo, K. Asano, M. Ohfuti, H. Kawarada, T. Sakai, M. Nihei, and Y. Awano, "Robustness of CNT via interconnect fabricated by low temperature process over a high-density current," in *Proc. IEEE IITC*, Jun. 2008, pp. 237–239.
- [10] H. Li, C. Xu, N. Srivastava, and K. Banerjee, "Carbon nanomaterials for next-generation interconnects and passives: Physics, status, and prospects," *IEEE Trans. Electron Devices*, vol. 56, no. 9, pp. 1799–1821, Sep. 2009.
- [11] H. Li, W. Y. Yin, K. Banerjee, and J. F. Mao, "Circuit modeling and performance analysis of multi-walled carbon nanotube interconnects," *IEEE Trans. Electron Devices*, vol. 55, no. 6, pp. 1328–1337, Jun. 2008.
- [12] A. Naeemi and J. D. Meindl, "Design and performance modeling for single-walled carbon nanotubes as local, semiglobal, and global interconnects in gigascale integrated systems," *IEEE Trans. Electron Devices*, vol. 54, no. 1, pp. 26–37, Jan. 2007.
- [13] H. Li, W. Liu, A. M. Cassell, F. Kreupl, and K. Banerjee, "Low-resistivity long-length horizontal carbon nanotube bundles for interconnect applications. Part I: Process development," *IEEE Trans. Electron Devices*, vol. 60, no. 9, pp. 2862–2869, Sep. 2013.
- [14] F. Yan, C. Zhang, D. Cott, G. Zhong, and J. Robertson, "High-density growth of horizontally aligned carbon nanotubes for interconnects," *Solid State Phys.*, vol. 247, pp. 2669–2672, Dec. 2010.
- [15] Y. Hayamizu, T. Yamada, K. Mizuno, R. C. Davis, D. N. Futaba, M. Yumura, and K. Hata, "Integrated three-dimensional microelectro-mechanical devices from processable carbon nanotube wafers," *Nature Nanotechnol.*, vol. 3, pp. 289–294, May 2008.
- [16] S. Tawfick, K. O'Brien, and A. J. Hart, "Flexible high-conductivity carbon-nanotube interconnects made by rolling and printing," *Small*, vol. 5, pp. 2467–2473, Nov. 2009.

- [17] M. H. Sun, Z. Y. Xiao, Y. Chai, Y. A. Li, and P. C. H. Chan, "Inductance properties of in situ-grown horizontally aligned carbon nanotubes," *IEEE Trans. Electron Devices*, vol. 58, no. 1, pp. 229–235, Jan. 2011.
- [18] N. Behabtu, C. C. Young, D. E. Tsentelovich, O. Kleinerman, X. Wang, A. W. K. Ma, E. A. Bengio, R. F. Ter Waarbeek, J. J. De Jong, R. E. Hoogerwerf, S. B. Fairchild, J. B. Ferguson, B. Maruyama, J. Kono, Y. Talmon, Y. Cohen, M. J. Otto, and M. Pasquali, "Strong, light, multifunctional fibers of carbon nanotubes with ultrahigh conductivity," *Science*, vol. 339, no. 6116, pp. 182–186, Jan. 2013.
- [19] H. Li and K. Banerjee, "High-frequency analysis of carbon nanotube interconnects and implications for on-chip inductor design," *IEEE Trans. Electron Devices*, vol. 56, no. 10, pp. 2202–2214, Oct. 2009.
- [20] G. D. Nessim, A. J. Hart, J. S. Kim, D. Acquaviva, J. Oh, C. D. Morgan, M. Seita, J. S. Leib, and C. V. Thompson, "Tuning of vertically-aligned carbon nanotube diameter and areal density through catalyst pre-treatment," *Nano Lett.*, vol. 8, no. 11, pp. 3587–3593, 2008.
- [21] Y. Pan, Y. Liu, W. Chi, and Z. Shen, "Inner-diameter enlargement of multi-walled carbon nanotubes by adding  $\text{HBO}_3$  in catalyst," *Mater. Lett.*, vol. 65, nos. 23–24, pp. 3362–3364, 2011.
- [22] A. R. Harutyunyan, G. Chen, T. M. Paronyan, E. M. Pigos, O. A. Kuznetsov, K. Hewaparakrama, S. M. Kim, D. Zakharov, E. A. Stach, and G. U. Sumanasekera, "Preferential growth of single-walled carbon nanotubes with metallic conductivity," *Science*, vol. 326, pp. 116–120, Oct. 2009.
- [23] J. Dijon, A. Fournier, P. D. Szkutnik, H. Okuno, C. Jayet, and M. Fayolle, "Carbon nanotubes for interconnects in future integrated circuits: The challenge of the density," *Diamond Rel. Mater.*, vol. 19, nos. 5–6, pp. 382–288, 2010.
- [24] G. Zhong, J. Warner, M. Fouquet, A. W. Robertson, B. Chen, and J. Robertson, "Growth of ultrahigh density single-walled carbon nanotube forests by improved catalyst design," *ACS Nano*, vol. 6, no. 4, pp. 2893–2903, 2012.
- [25] S. Sato, M. Nihei, A. Mimura, A. Kawabata, D. Kondo, H. Shioya, T. Iwai, M. Mishima, M. Ohfuti, and Y. Awano, "Novel approach to fabricating carbon nanotube via interconnects using size-controlled catalyst nanoparticles," in *Proc. IEEE IITC*, Jun. 2006, pp. 230–232.
- [26] C. L. Pint, Y.-Q. Xu, M. Pasquali, and R. Hauge, "Formation of highly dense aligned ribbons and ultra-thin films of single-walled carbon nanotubes from carpets," *ACS Nano*, vol. 2, no. 9, pp. 1871–1878, 2008.
- [27] A. Naemi and J. D. Meindl, "Physical modeling of temperature coefficient of resistance for single- and multi-wall carbon nanotube interconnects," *IEEE Electron Device Lett.*, vol. 28, no. 2, pp. 135–138, Feb. 2007.
- [28] H. Li, N. Srivastava, J.-F. Mao, W.-Y. Yin, and K. Banerjee, "Carbon nanotube vias: A reality check," in *IEDM Tech. Dig.*, 2007, pp. 207–210.
- [29] K. Banerjee and A. Mehrotra, "Global (interconnect) warming," *IEEE Circuits Devices Mag.*, vol. 17, no. 5, pp. 16–32, Sep. 2001.
- [30] T. Kawano, H. C. Chiamori, M. Suter, Q. Zhou, B. D. Sosnowchik, and L. Lin, "An electrothermal carbon nanotube gas sensor," *Nano Lett.*, vol. 7, no. 12, pp. 3686–3690, 2007.
- [31] S. Im, N. Srivastava, K. Banerjee, and K. E. Goodson, "Scaling analysis of multilevel interconnect temperatures for high performance ICs," *IEEE Trans. Elect. Device*, vol. 52, no. 12, pp. 2710–2719, Dec. 2005.
- [32] E. Pop, "The role of electrical and thermal contact resistance for joule breakdown of single-wall carbon nanotubes," *Nanotechnology*, vol. 19, no. 29, p. 295202, 2008.
- [33] K. Hata, D. N. Futaba, K. Mizuno, T. Namai, M. Yumura, and S. Iijima, "Water-assisted highly efficient synthesis of impurity-free single-walled carbon nanotubes," *Science*, vol. 306, no. 5700, pp. 1362–1364, 2004.



**Hong Li** (S'07–M'12) received the Ph.D. degree in electrical and computer engineering from the University of California, Santa Barbara, CA, USA, in 2012.

He is currently an Emerging Memory Engineer with Micron Technology Inc., Boise, ID, USA.



**Wei Liu** (M'10) received the Ph.D. degree in chemistry from the Institute of Chemistry, Chinese Academy of Sciences, Beijing, China, in 2008.

He is currently a Post-Doctoral Research Scholar with the University of California, Santa Barbara, CA, USA.



**Alan M. Cassell** received the Ph.D. degree in materials chemistry from the University of South Carolina, Columbia, SC, USA, in 1998.

He is currently an Aerospace Engineer with the Entry Systems and Vehicle Development Branch, NASA Ames Research Center.



**Franz Kreupl** (M'04) is a Professor of electrical engineering with Technische Universitat Muenchen, Muenchen, Germany.



**Kaustav Banerjee** (S'92–M'99–SM'03–F'12) is a Professor of electrical and computer engineering with the University of California, Santa Barbara, CA, USA.